Numerical simulation of particle dispersion in the developing supersonic mixing layer

ALTYN MAKASHEVA[1], ALTYNSHASH NAIMANOVA [2]

1. Institute of Mathematics and Mathematical Modeling, Almaty, Kazakhstan
(e-mail: altyn-mak@mail.ru)
2. Institute of Mathematics and Mathematical Modeling, Almaty, Kazakhstan
(e-mail: alt_naimanova@yahoo.com).

Abstract— The work is devoted to the numerical simulation of a supersonic planar mixing layer of multispecies gases with the particles injection at the interface of flows. It is assumed that the turbulent flow is quasi-two-dimensional, and the solution of the Navier-Stokes equations for multispecies gaseous phase is performed with the 2D-DNS (Direct Numerical Simulations) approach, and the system of ordinary differential equations for solid particles is used. The supersonic multispecies gases effect to the dispersion of particles in the range of $20 \le d_p \le 200$ is studied in detail. The obtained results show the small particles are captured by the vortices homogeneously while the large particles are accumulated in the periphery of the vortices and along the braid of two adjacent vortices. The dispersion of the particles in supersonic multispecies mixture layer is similar to the trajectory of the particles in subsonic flow: the large particles reacted to the centrifugal action, while the small particles are in a quasi-equilibrium status with the gases. And the number of the particles is larger in the high speed hydrogen than in the air flow.

Keywords – mixing layer, particle dispersion, multispecies gases, Lagrangian approach, large and small particles.

1 Introduction

The problem of the spatial supersonic mixing layer is important both theoretically and practically in connection with its wide engineering applications. Many experiments have been conducted [1, 2] in area of compressible free shear layers, where it was demonstrated that the growth rate of mixing layer decreases with increase of the convective Mach number. Numerically, turbulent mixing layers have been successfully studied for the wide range of the convective Mach numbers for subsonic [3, 4] and supersonic [5, 6] flows.

Many efficient technologies of the industry deal with mixing layers in presence of particles. Nowadays, the dispersed phase with particles in a two-phase flow (solid, droplet or bubble suspensions) is studied as experimentally [7-9] as numerically [10-13]. An influence of the large-scale turbulent structures of the planar mixing layer to the particle dispersion and its correlation has been studied in [7-9].

There are two approaches in numerical study of a two-phase flow. In the first method, discrete elements are tracked through a continuous fluid by solving the system of ordinary equations for each element (Eulerian-Lagrangian approach). In the second methodology (Eulerian-Eulerian approach), both phases are considered as two continuums and are governed by the fluid dynamics equations. Comparing these two approaches, it should be noted, that the numerical models based on the Euler-Lagrangian approach of the two-phase flow allow performing detailed study of the flow physics of gases as well as particles and their interaction.

Euler-Lagrangian method has been used in [9] for simulation of a small spherical solid particles in the shear turbulent flows and it was found that particles mainly disperse in the streamwise direction due to the shear effect.

Review of numerical studies of the influence of vortex structures in the spatially-developed shear layer on the particle dynamics for the low Mach number regime is given in [10], and the influence on the particle dispersion for different size of particles is represented in [11].

A limited number of studies on the dynamics of the large number of particles in the supersonic flows has been performed [14, 15]. Usually, these flows have complicated flow structures, such as compression waves and expansion waves, which can affect the particle dispersion (the dispersion of emissions from jet engines). In addition, for such flows the influence of the gas compressibility on

particles is also important. For example, the numerical simulation of the supersonic flows considering compressibility effects was carried out in [14], where an injection of droplets with the transverse-jet was investigated.

In accordance with the above, the study of the supersonic multispecies mixing layers flow models will be developed to obtain a field of the gas (carrier fluid) and its influence on the dispersion of both small and large particles of range $20 \le d_p \le 200$. The inflow profile of physical parameters across the hydrogen-nitrogen and air flows is assumed to vary smoothly according to a hyperbolic-tangent function (Fig. 1). At the entrance, the solid particles with random size are injected to the mixing layer. The investigation focuses on the influence of a spatially developing vortex structures on a particle dispersion in a transitional free shear layer depending on the particle size.

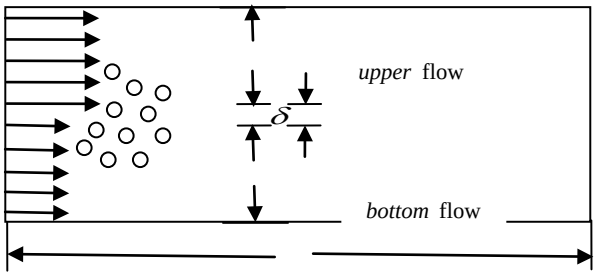

Fig. 1 illustration the flow configuration

2 The mathematical model and governing equations

2.1 Governing equations for continuous phase

The carrier gas is considered in the Navier-Stokes equations for multi-species gas which are written in the conservation vector form as:

$$\frac{\partial \vec{U}}{\partial t} + \frac{\partial\left(\vec{E} - \vec{E}_v\right)}{\partial x} + \frac{\partial\left(\vec{F} - \vec{F}_v\right)}{\partial z} = 0, \qquad (1)$$

Vectors $\vec{U}, \vec{E}, \vec{F}$ are defined by

$$\vec{U} = \begin{pmatrix} \rho \\ \rho u \\ \rho w \\ E_t \\ \rho Y_k \end{pmatrix}, \quad \vec{E} = \begin{pmatrix} \rho u \\ \rho u^2 + p \\ \rho uw \\ (E_t + p)u \\ \rho u Y_k \end{pmatrix}, \quad \vec{F} = \begin{pmatrix} \rho w \\ \rho uw \\ \rho w^2 + p \\ (E_t + p)w \\ \rho w Y_k \end{pmatrix},$$

and vectors $\vec{E}_v, \vec{F}_v$ are associated with viscous stress

$$\vec{E}_v = \begin{pmatrix} 0 \\ \tau_{xx} \\ \tau_{xz} \\ u\tau_{xx} + w\tau_{xz} - q_x \\ J_{kx} \end{pmatrix}, \quad \vec{F}_v = \begin{pmatrix} 0 \\ \tau_{xz} \\ \tau_{zz} \\ u\tau_{xz} + w\tau_{zz} - q_z \\ J_{kz} \end{pmatrix}.$$

The components of the viscous stress tensor are given as

$$\tau_{xx} = \frac{\mu}{\mathrm{Re}}\left(2u_x - \frac{2}{3}(u_x + w_z)\right); \quad \tau_{zz} = \frac{\mu}{\mathrm{Re}}\left(2w_z - \frac{2}{3}(u_x + w_z)\right);$$

$$\tau_{xz} = \tau_{zx} = \frac{\mu}{\mathrm{Re}}(u_z + w_x);$$

The heat flux is defined by

$$q_x = \frac{1}{\mathrm{Pr}\,\mathrm{Re}}\left(\mu + \frac{\mu}{\sigma_k}\right)\frac{\partial T}{\partial x}; \quad q_z = \frac{1}{\mathrm{Pr}\,\mathrm{Re}}\left(\mu + \frac{\mu}{\sigma_k}\right)\frac{\partial T}{\partial z};$$

and the diffusion flux is determined by

$$J_{kx} = -\frac{\mu_l}{Sc\mathrm{Re}}\frac{\partial Y_k}{\partial x}, \quad J_{kz} = -\frac{\mu_l}{Sc\mathrm{Re}}\frac{\partial Y_k}{\partial z}.$$

The pressure, the total energy are given by

$$p = \frac{\rho T}{\gamma_\infty M_\infty^2}\left(\sum_{k=1}^{N}\frac{Y_k}{W_k}\right),$$

$$E_t = \frac{\rho h}{\gamma_\infty M_\infty^2} - p + \frac{1}{2}\rho\left(u^2 + w^2\right),$$

The specific enthalpy and the specific heat at constant pressure of the k^{th} species are

$$h = \sum_{k=1}^{N} Y_k h_k, \quad h_k = h_k^0 + \int_{T_0}^{T} c_{pk}\,dT,$$

$$c_{pk} = C_{pk}/W, \quad C_{pk} = \sum_{i=1}^{5} \overline{a}_{ki} T^{(i-1)},$$

$$\overline{a}_{jk} = a_{jk} T_{\infty}^{\,j-1}$$

where the molar specific heat C_{pk} is given in terms of the fourth degree polynomial with respect to the temperature, consistent with the JANAF Thermochemical Tables [13].

In the system (1) u, w, ρ, T represent the components of the velocity vector, the density and the temperature, respectively. Y_k and W_k are the mass fraction and the molecular weight of the k^{th} species, $k = 1...N$, where N is the number of components in a gas mixture. τ, q and J_k are the viscous stress tensor, the heat flux and the diffusion flux, respectively. Re is the Reynolds number, Pr is the Prandtl number, Sc is the Schmidt number, μ_l is the molecular viscosity calculated by Wilke formula [16].

The system of equations (1) is written in the conservative, dimensionless form. The air flow parameters are $\rho_{\infty}, u_{\infty}, w_{\infty}, T_{\infty}$, the hydrogen jet parameters are ρ_0, u_0, w_0, T_0. In terms of dimensionless variables $\rho_{\infty} u_{\infty}^2$ is the scale, $R_0 T_{\infty}/W_{\infty}$ is the enthalpy scale, R_0 is the molar specific heat scale and δ (the thickness of the splitter plate) is the spatial distance.

2.2 Governing equations of discrete phase

The small sphere particles are tracked individually in the Lagrangian manner. It is assumed that the density of particles is much larger than that of the continuous phase so only the drag force is significant. The particle collision is neglected.

The Lagrangian particle equations for position and velocity are given by

$$\begin{cases} \dfrac{d}{dt}\vec{x}_p = \vec{u}_p \\ \dfrac{d}{dt}\vec{u}_p = D_p\left(\vec{u} - \vec{u}_p\right) \end{cases} \tag{2}$$

Here, $\vec{x}_p$ is the particle position vector, $\vec{u}_p$ is the particle velocity vector; D_p is the drag force with the particle radius r_p is given by

$$D_p = \frac{3}{8}\frac{\rho}{\rho_p}\frac{\left|\vec{u} - \vec{u}_p\right|}{r_p} C_D\left(Re_p\right)$$

The drag coefficient C_D is taken in accordance with the solid sphere drag correlation [17]:

$$C_D = \begin{cases} \dfrac{24}{Re_p}\left(1 + \dfrac{1}{6}Re_p^{2/3}\right), & Re_p \le 1000 \\ 0{,}424, & Re_p > 1000 \end{cases}$$

and $Re_p = \dfrac{2\rho\left|\vec{u} - \vec{u}_p\right| \cdot r_p}{\mu}$ is the particle Reynolds number, μ is the gas viscosity.

3 Initial and boundary conditions

At the entrance:

- for multi-species gas:

bottom flow:

$$u = M_0\sqrt{\frac{\gamma_0 R_0 T_0}{W_0}}, \quad w = 0, \quad p = p_0, \quad T = T_0,$$

$Y_k = Y_{k0}$ at $x = 0$, $0 \le z < \mathrm{H}_1$.

upper flow:

$$u = M_{\infty}\sqrt{\frac{\gamma_{\infty} R_0 T_{\infty}}{W_{\infty}}}, w = 0, \quad p = p_{\infty}, \quad T = T_{\infty},$$

$Y_k = Y_{k\infty}$ at $x = 0$, $\mathrm{H}_1 + \delta \le z \le \mathrm{H}_2$.

At the point of transition of two gas flows, the above physical variables are determined by the function of the hyperbolic tangent

$$\phi(\mathrm{z}) = 0.5\left(\phi_0 + \phi_{\infty}\right) + 0.5\left(\phi_0 - \phi_{\infty}\right)\tanh\left(0.5z/\delta_{\theta}\right)$$

at $x = 0$, $0 \le z \le H$, $\phi = (u, w, Y_k, T)$

where

$$\delta_{\theta}(x) = \int_{H_1/2}^{H_2/2}\left(\rho\left(\tilde{u} - u_{\infty}\right)\left(u_0 - \tilde{u}\right)/\left(\rho_{\infty}\Delta u^2\right)dz\right)$$ is the momentum thickness, $\tilde{u} = \left(u - u_{\infty}\right)/\Delta u$ is the average of gas velocity.

On the lower and upper boundaries, the condition of symmetry is imposed. At the outflow, the non-reflecting boundary condition is used [18].

In order to produce the roll-up and pairing of vortex rings, an unsteady boundary condition for velocity field is used at the inlet plane [19], i.e.

$\phi = \phi(z) + \phi_{distr}$,

$$\phi_{distr} = \begin{cases} A \cdot \Delta U \cdot \cos(\omega \cdot t + \alpha) \\ A \cdot \Delta \mathrm{U} \cdot \mathrm{Gaussian(z)} \cdot \sum_{\mathrm{m}=0}^{3} \sin(2\pi f_m \cdot t + \alpha) \end{cases}$$

where $\phi(z)$ is the hyperbolic-tangent velocity profile defined by (3). Coefficient $A = 0.001$ is the forcing amplitude. $\Delta U = (u_\infty - u_0)$ is the difference between the two stream velocities, which measures the strength of shearing. $\omega = (a_0 + a_\infty)/(2\delta_\theta)$ is the disturbance frequency, $Gaussian(z) = \exp(-z^2/2\sigma^2)$ is the Gaussian function which has a peak value of a unity at z=0 and the width $\pm 2\sigma$ is matched to the vorticity layer thickness at the entrance. The Δw_{factor} is taken as in [18]. The ω is the excitation frequency, $\delta_w = \frac{(u_\infty - u_0)}{(\partial u/\partial z)_{\max}}$ is the vorticity thickness, a_0, a_∞ are the sound velocities, α is the random phase.

4 Method of solution

The numerical solution of quasi-2D equations is performed in two steps. Where, in the first-step the gas dynamic parameters (ρ, u, w, E_t) and species ($Y_k, k = 1,...,7$) with mass source terms are solved. In the second-step, the system of ordinary equation for particles is calculated.

The system of equations (1) in the new coordinate system is written as

$$\frac{\partial \vec{U}}{\partial t} + \frac{\partial \vec{E}}{\partial \xi} + \frac{\partial \vec{F}}{\partial \eta} = \frac{\partial \vec{E}_{v2}}{\partial \xi} + \frac{\partial \vec{E}_{vm}}{\partial \xi} + \frac{\partial \vec{F}_{v2}}{\partial \eta} + \frac{\partial \vec{F}_{vm}}{\partial \eta} \qquad (4)$$

where $\widetilde{U} = \widetilde{U}/J$, $\vec{E} = \xi_x \vec{F}/J$, $\widetilde{F} = \eta_z \widetilde{F}/J$, $\widetilde{E}_{v2} = \xi_x \widetilde{E}_{v2}/J$, $\vec{E}_{vm} = \xi_x \vec{E}_{vm}/J$, $\widetilde{F}_{v2} = \eta_z \widetilde{F}_{v2}/J$, $\widetilde{F}_{vm} = \eta_z \widetilde{F}_{vm}/J$, $J = \partial(\xi,\eta)/\partial(x,z)$ is the Jacobian transformation.

The system (4) is solved with semi-implicit method, numerical algorithm is given in detail in [20,21]. In accordance with the principle of the ENO scheme, the system (4) is written formally as

$$\frac{\partial \widetilde{U}}{\partial t} + (A^+ + A^-)\frac{\partial E^m}{\partial \xi} + (B^+ + B^-)\frac{\partial F^m}{\partial \eta} -$$

$$-\left[\frac{\partial(\widetilde{E}_{v1} + \widetilde{E}_{vm})}{\partial \xi} + \frac{\partial(\widetilde{F}_{v2} + \widetilde{F}_{vm})}{\partial \eta}\right] = 0 \qquad (5)$$

Here E^m and F^m are the modified fluxes at node points (i, j) which consist of the original advection $(\widetilde{E}, \widetilde{F})$ and additional terms of third-order accuracy $(\widetilde{E}_\xi, \widetilde{D}_\xi, \widetilde{E}_\eta, \widetilde{D}_\eta,)$: $\widetilde{E}^m = \widetilde{E}^{n+1} + (\widetilde{E}_\xi + \widetilde{D}_\xi)^n$, and $A^+ + A^- = I$, $\hat{A}^\pm = A^\pm A^{-1}$, $A^\pm = R\Lambda^\pm R^{-1} = R\left(\frac{\Lambda \pm |\Lambda|}{2}\right)R^{-1}$, I is the identity matrix. $A = \partial\vec{E}/\partial\vec{U}$ is the Jacobi matrix, R and R^{-1} are the left and the right eigenvectors, Λ is the matrix of eigenvalues.

The system (5) is transformed into one – dimensional operators after factorization:
1st step:

$$\left[I + \Delta t\left\{\left(\hat{A}^+_{i-1/2}\Delta_- A^n_\xi + \hat{A}^-_{i+1/2}\Delta_+ A^n_\xi\right) + \Delta\frac{\mu_t \xi_x^2}{\mathrm{Re}\, J}\Delta\frac{1}{U_1^n}\right\}\right]\mathrm{U}^* = RHS^n_\xi + RHS^n_\eta$$

2nd step: (6)

$$\left[I + \Delta t\left\{\left(\hat{B}^+_{j-1/2}\Delta_- B^n_\eta + \hat{B}^-_{j+1/2}\Delta_+ B^n_\eta\right) + \Delta\frac{\mu_t \eta_z^2}{\mathrm{Re}\, J}\Delta\frac{1}{U_1^n}\right\}\right]\tilde{\mathrm{U}}^{n+1} = \mathrm{U}^*$$

$$RHS^n_\xi = \hat{A}^-_{i+1/2\,j}\left[\left(\vec{E}_\xi + \vec{D}_\xi\right)_{i+1\,j} - \left(\vec{E}_\xi + \vec{D}_\xi\right)_{i\,j}\right]^n + \hat{A}^+_{i-1/2\,j}\left[\left(\vec{E}_\xi + \vec{D}_\xi\right)_{i\,j} - \left(\vec{E}_\xi + \vec{D}_\xi\right)_{i-1\,j}\right]^n$$

$$\hat{A}^-_{i+1/2\,j}\left[\left(\vec{E}_\xi + \vec{D}_\xi\right)_{i\,j}\right]^n =$$

$$= R\,\hat{\Lambda}^-\,R^{-1}_{i+1/2\,j}\Big(\textbf{\textit{minmod}}\left(\overline{E}_{\xi\,i+1/2\,j}\;\overline{E}_{\xi\,i-1/2\,j}\right) + \begin{cases} \dot{m}\left(\Delta_-\hat{D}_{\xi\,i+1/2\,j},\ \Delta_+\hat{D}_{\xi\,i+1/2\,j}\right) & \text{if } \left|\Delta_-\widetilde{U}_{ij}\right| > \left|\Delta_+\widetilde{U}_{ij}\right| \\ \dot{m}\left(\Delta_-\overline{D}_{\xi\,i-1/2\,j},\ \Delta_+\overline{D}_{\xi\,i-1/2\,j}\right) & \text{if } \left|\Delta_-\widetilde{U}_{ij}\right| \le \left|\Delta_+\widetilde{U}_{ij}\right| \end{cases}\Big)$$

$$\hat{A}^+_{i-1/2\,j}\left[\left(\vec{E}_\xi + \vec{D}_\xi\right)_{i\,j}\right]^n =$$

$$= R\,\hat{\Lambda}^+\,R^{-1}_{i-1/2\,j}\Big[\Big(\textbf{\textit{minmod}}\left(\overline{E}_{\xi\,i+1/2\,j}\;\overline{E}_{\xi\,i-1/2\,j}\right) -$$

$$-\left\{\begin{array}{ll}\dot{m}\left(\Delta_{-}\hat{D}_{\xi i-1/2j},\ \Delta_{+}\hat{D}_{\xi i-1/2j}\right) & if\quad \left|\Delta_{-}\tilde{U}_{ij}\right|\le\left|\Delta_{+}\tilde{U}_{ij}\right| \\ \dot{m}\left(\Delta_{-}\overline{D}_{\xi i-1/2j},\ \Delta_{+}\overline{D}_{\xi i-1/2j}\right) & if\quad \left|\Delta_{-}\tilde{U}_{ij}\right|\le\left|\Delta_{+}\tilde{U}_{ij}\right|\end{array}\right)\Bigg]$$

$$\overline{E}_{\xi i\pm1/2j}=\left(R\,sign(\Lambda)R^{-1}\right)_{i\pm1/2j}\cdot$$
$$\cdot\frac{1}{2}\left[I-\frac{\Delta t}{\Delta\xi}\left(R\left|\Lambda\right|R^{-1}\right)_{i\pm1/2}\right]\Delta_{\pm}\tilde{E}_{ij}$$

$$\overline{D}_{\xi i\pm1/2j}=\left(R\,sign(\Lambda)R^{-1}\right)_{i\pm1/2j}\cdot$$
$$\cdot\frac{1}{6}\left[\frac{\Delta t^2}{\Delta\xi^2}\left(R\left|\Lambda\right|R^{-1}\right)^2_{\pm}-I\right]\Delta_{\pm}\tilde{E}_{ij}$$

$$\hat{D}_{\xi i\pm1/2j}=\overline{E}_{\xi i\pm1/2j}+\overline{D}_{\xi i\pm1/2j}$$

where

$$\textbf{\textit{minmod}}(a,b)=\begin{cases}s\cdot min\left(|a|,|b|\right), & if\quad sign(a)=sign(b)=s\\ 0, & \text{otherwise}\end{cases}$$

$$\dot{m}(a,b)=\begin{cases}a & if\quad |a|\le|b|\\ b & if\quad |a|>|b|\end{cases}$$

The second item $RHS^n{}_\eta$ is written similarly.

The system (6) is solved with respect to the vector of thermodynamic parameters by the matrix sweep method, and the vector of mass fractions of the mixture is computed with tridiagonal inversion.

5 Result and discussion

The parameters of coordinate transformation are as follows:

$$\xi(x)=K+\frac{1}{r}arsh\left[\left(\frac{x}{x_\eta}-1\right)sh(\tau K)\right],$$

$$\eta(z)=H\left[(\beta+1)-(\beta-1)\left(\frac{\beta+1}{\beta-1}\right)^{1-\frac{z}{a}}\right]\div$$

$$\div\left[\left(\frac{\beta+1}{\beta-1}\right)^{1-\frac{z}{a}}+1\right]$$

$$K=\frac{1}{2\tau}\ln\left[\left(1+\left(e^{x}-1\right)\frac{x_c}{L}\right)\Big/\left(1-\left(e^{x}-1\right)\frac{x_c}{L}\right)\right],\ \beta,\ \tau$$

are the clustering coefficients with β, $\tau>1$, a is the computational region height in the new coordinate system, and x_c is the point with respect to which the clustering is done.

The free shear layer of a hydrogen-air flows mixing with injection of a solid particles is numerically studied. The initial momentum thickness is $\delta_\theta=9.35x10^{-5}\ m$. The algorithm of method and the sensitivity of convergence of solutions to the grid characteristics were studied in detail in [20, 21]. The dimensionless length and height of area under consideration are LxH = 600x80. Here the 526x201 nodes grid with the stretching at the entrance and the mixing layer is used.

Numerical simulationis performed the initial parameters on the bottom and upper flow: $M_0=2.1$, $M_\infty=2.0$ $T_0=T_\infty=2000\ K$, $p_0=p_\infty=101325\ Pa$. At the same time, the convective Mach number is $M_c=0.38$, where $M_c=\left(u_c-u_\infty\right)/a_\infty$, $u_c=\left(a_\infty u_0+a_0 u_\infty\right)/\left(a_\infty+a_0\right)$. At the inflow plane, the hydrogen-nitrogen mixture enters from the upper half: $Y_{H_2}=0.5$, $Y_{N_2}=0.5$ and the air $Y_{O_2}=0.2$, $Y_{N_2}=0.8$ enters from the lower half of the domain.

The particles are injected into the flow uniformly, one by one after the period of time $\Delta t=5$. The particle density and diameter are $\rho_{p0}=\rho_{p\infty}=2560kg/m^3$ and $20\,\mu m$, respectively. The aluminum particles are injected from four input points $x=0$, $z=20,30,40,50$.

The formation of vortex structures is shown on example of vortices isolines at different times t =200, 1000, 1500 (Fig. 2). From the Figure follows that to the time t = 200 isolines are starting to curve significantly and roll-up into vortices (Fig. 2a) and they are pairing with adjacent vortices to form larger ones downstream. As result of which, relatively stable turbulent vorticity fields are formed (Fig. 2c.)

The isolines of the hydrogen (Fig. 3) well demonstrate both, the dynamic of the formation and growth of a system of vortices, and the gases mixing. In accordance with the picture of vortices (Fig. 3a, to the time t=200), it can be seen that as a result of the rotation of a pair of vortices, both, the air flow and the hydrogen-nitrogen mixture are trapped by this pair. From numerical experiment follows that in result of increasing of twisting of vortices, as well as their pairing, in the centers of their rotation the closed zones of hydrogen are formed (Fig. 3b and 3c). It follows from the figure that the mixing layer expands towards the slow air flow.

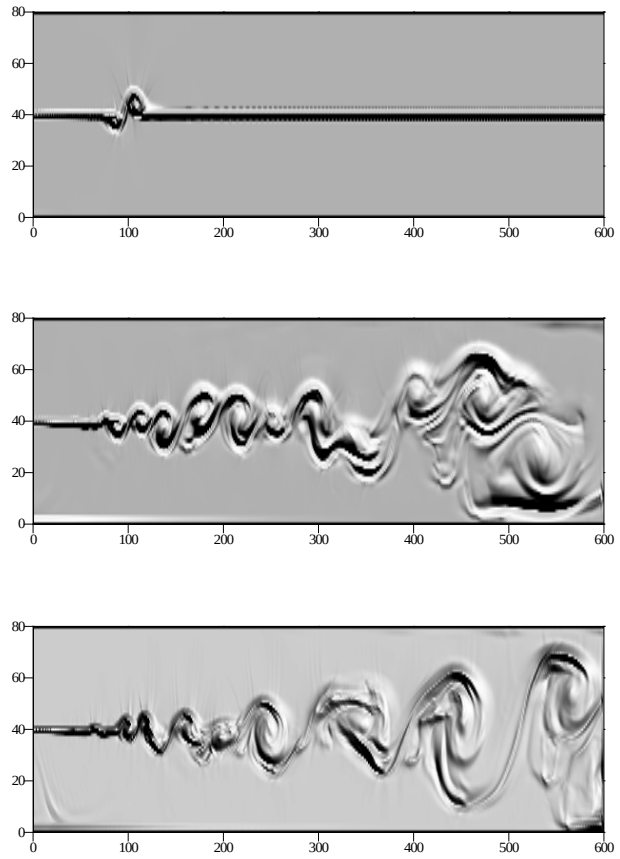

Fig. 2 The formation of vortex structures at time: a) $t = 200$, b) $t = 1000$, c) $t = 1500$ for $d_p = 20$ *mkm* $M_0 = 2.1$, $M_\infty = 2$

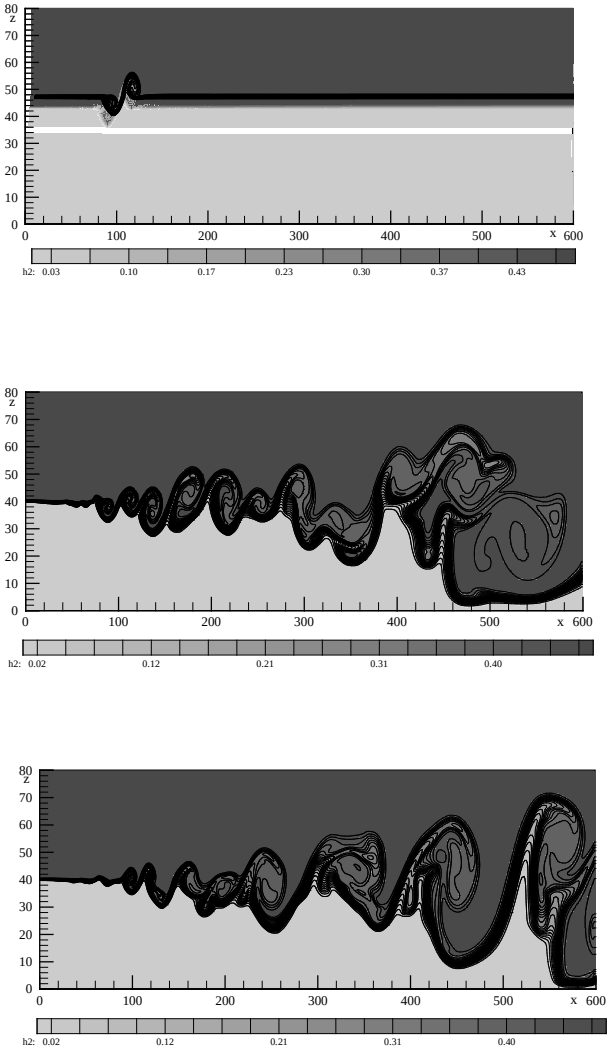

Fig. 3 Isolines of hydrogen at time: a) $t = 200$, b) $t = 1000$, c) $t = 1500$ for $d_p = 20$ *mkm* $M_0 = 2.1$, $M_\infty = 2$

Below represented the dynamics of particles and their entrapping with multispecies gases (Figure 4, t=200, 1000, 1500). From the graphs is visible that the particles injected into the faster flow (z=40, 50) of mixing layer move much faster compared to those injected into the slower flow (z =20, 30). For example, particles injected into the upper stream to the time (Fig. 4a) extend up to x=200. At the same time t=200, some of them get into vortex zone, and as result their trajectories are curved significantly. Whereas the particles injected from a lower stream are not captured by the vortices yet, they continue to move along their own trajectories and by the time they reach the position of x=90.

From graph 4b and 4c it can be seen in spite of that the particles are homogeneously entrapped by the vortices including vortex core, the dispersion of particles injected into a slower flow is much smaller compared to particles which move in a faster flow.

Numerical experiments performed with particles of the large particle diameter $d_p = 200\,\mu m$ show another picture of particles distribution in the mixing layer.

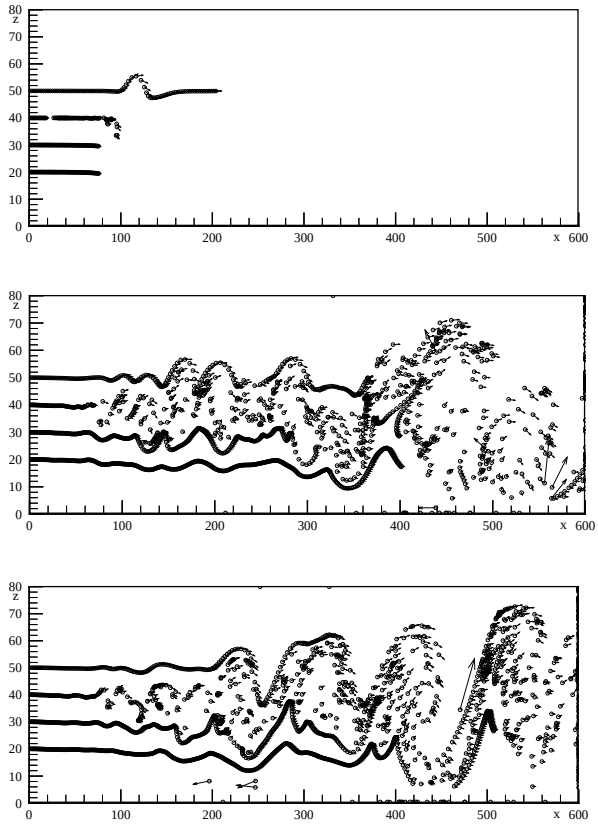

Fig. 4 Distribution of particles at time: a) $t = 200$, b) $t = 1000$, c) $t = 1500$ for $d_p = 20$ *mkm* $M_0 = 2.1$, $M_\infty = 2$

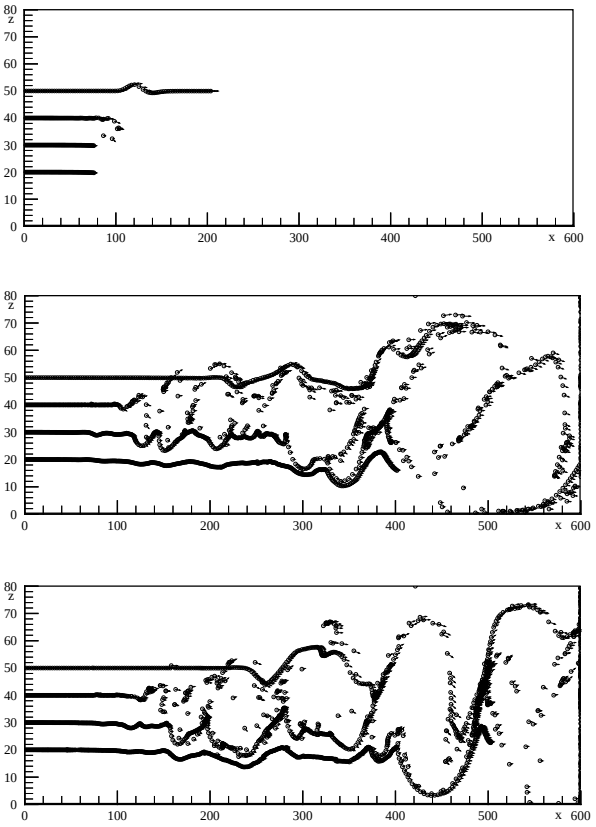

Fig. 5 Distribution of particles at time: a) $t = 200$, b) $t = 1000$, c) $t = 1500$ for $d_p = 200$ *mkm* $M_0 = 2.1$, $M_\infty = 2$

As it can be seen from Figure 5 in this case, a few particles reach the vortex core. Mainly, they are accumulated in the periphery of the vortices and along the braid of two adjacent vortices. Consequently, large particles are reacted to the centrifugal action, while small particles are in a quasi-equilibrium status with the gases.

Numerical experiments show that the behavior of the dispersion of large particles in a supersonic mixing layer are in qualitative agreement with the observed behavior of particles in a subsonic mixing layer [13, 22].

Figure 6 shows the quantitative distribution of the numbers of small particles in the upper ($z \in [40,80]$, Fig. 6a) and the lower ($z \in [0,40)$, Fig. 6b) part of the mixing layer along the streamwise direction to the time t=1500, which is defined as follows:

$$N_{rms}(x) = \left(\sum_{i=1}^{N_{cp}} \frac{N_i(x)^2}{N_{cp}} \right)^{1/2}$$

here N_{cp} is the total number of computational cells, and $N_i(x)$ is the number of particles in the i cell. As can be seen from the figure in accordance with the pattern of expansion of the mixing layer the number of small particles in the lower air flow (Fig. 6a) is larger compared to the upper hydrogen-nitrogen mixture (Fig. 6b).

The picture of the distribution of the large particles show that in main, the total number of them coincide with small particles, exclude the region of large vortex structures ($x = 450 \div 500$, Fig. 7).

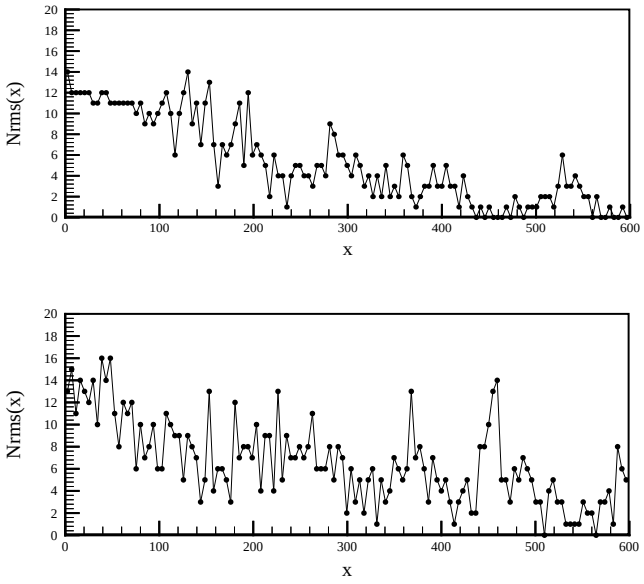

Fig. 6 Quantitative distribution of the number of particles in the upper (a) and lower (b) of mixing layers
at $t = 1500$ for $d_p = 20$ *mkm*
$M_0 = 2.1,\ M_\infty = 2$

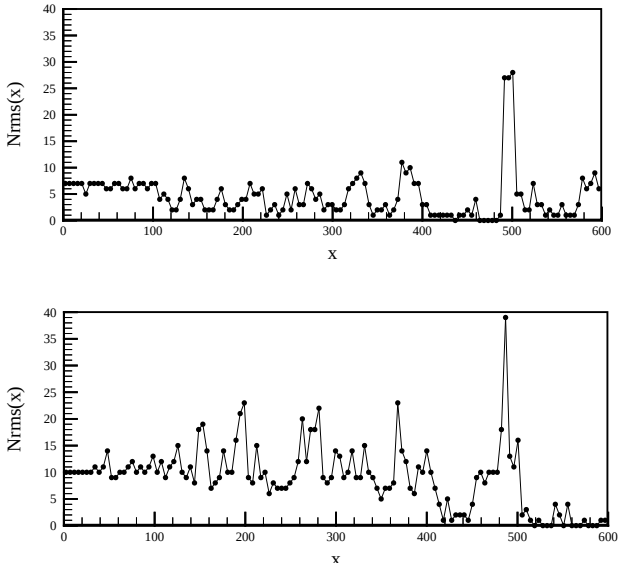

Fig. 7 Quantitative distribution of the number of particles in the upper (a) and lower (b) of mixing layer at $t = 1500$ for $d_p = 200$ *mkm*
$M_0 = 2.1,\ M_\infty = 2$

References:

[1] Wygnanski, I., Weisbrot, I. On the pairing process in an excited plan turbulent mixing layer, J. Fluid Mech., pp.161–173, 1998, vol.195.

[2] Goebel S.G., Dutton J.C. Experimental study of compressible turbulent mixing layers, AIAA Journal, pp. 538-546, 1991, vol. 29, №4.

[3] Grinstein S, Mills G.B, Cheng R.K, Cragoe E.J, Gelfand E.W. Activation of the NA^+/H^+antiport is not required for lectin-induced proliferation of human T-lymphocytes, Journal Immunol, pp. 1150-1154, 1986, vol. 136.

[4] Pantano C., Sarkar S. A Study of Compressibility Effects in the High-Speed, Turbulent Shear Layer using Direct Sim., J. Fluid Mechanics, pp. 329–371, 2002, vol. 451.

[5] Sarkar S. The stabilizing effect of compressibility in turbulent shear flow, Journal Fluid Mechanics, pp. 163–186, 1995, vol. 282.

[6] Papamoschou D. Structure of the compressible turbulent shear layer, AIAA Journal, pp. 126-135, 1989, vol. 89.

[7] Balaras E., Piomelli U., Wallace J.M. Self-similar states in turbulent mixing layers, Journal Fluid Mechanics, pp. 1-24, 2001, vol. 446.

[8] Lazaro B. J. and Lasheras J. C. Particle dispersion in the developing free shear layer. Part 1, Journal Fluid Mechanics, pp. 235-247, 1992, vol.143.

[9] Lazaro B. J. and Lasheras J. C. Particle dispersion in the developing free layer. Part 2, Journal Fluid Mechanics, pp. 179-185, 1992, vol. 235.

[10] Wang B., Ren Zh., Zhang H. Stochastic separated flow models with applications in num. computations of supersonic particle-laden turb. Flows, Mech. Engineering, pp.12-16, 2015.

[11] Wang Z.J. High-Order Methods for the Euler and Navier-Stokes Equations on Unstructured Grids, Progress in Aerospace Sciences, pp. 1-41, 2007, vol. 43.

[12] Jacobs G., Don W. S. and Dittmann T. High-Order Resolution Eulerian-Lagrangian Simulations of Particle Dispersion in the Accelerated Flow behind a Moving Shock, Theoretical and Computer Fluid Dynamics, pp. 1052-1069, 2010, vol.5.

[13] Aggarwal S.K., Yapo J.B., Grinstein F.F. and Kailasanath K. Numerical simulation of particle transport in planar shear layers, Computers and Fluids, pp. 39-59, 1996, vol. 25, № 1.

[14] Moser R.D., Rogers M.M. The three-dimensional evolution of a plane mixing layer: pairing and transition to turbulence, Journal Fluid Mechanics, pp. 275-320, 1993, vol. 247.

[15] Stanley S., Sarkar S. Simulation of spatially developing two-dimensional shear layer and jets, Theoretical Computer Fluid Dynamics, pp. 121-147, 1997, vol. 9.

[16] Wilcox D.C. Dilatation-dissipation corrections for advanced turbulence models, AIAA J., pp. 2639–2646, 1992, vol. 30.

[17] R. Chein and J.N. Chung "Effects of vortex pairing on particle dispersion in turbulent shear flows", Multiphase Flow, pp. 775-785, 1987, vol.13.

[18] T. Poinsot, S. Lele "Boundary Conditions for Direct Simulation of Compressible Viscous Flows", Computational Physics, pp. 104-129, 1992, vol.101

[19] H. Ounis and G. Ahmadi "Motions of small particles in a turbulent simple shear flow field under microgravity condition" Phys. Fluids A. pp.2559-2570, 1991, vol. 3.

[20] A. Beketaeva, A. Naimanova "Numerical study of spatial supersonic flow of a perfect gas with transverse injection of jets", Applied Mechanics and Technical Physics, pp. 896-904, 2011, vol.52.

[21] P. Bruel, A.Zh. Naimanova "Computation of the normal injection of a hydrogen jet into a supersonic air flow", Thermophysics and Aeromechenics, pp. 531-542, 2010, vol. 17, No. 4.

[22] Hu Zhiwei, Luo Xiaoyu, H. Luo Kai "Numerical Simulation of Particle Dispersion in a Spatially Developing Mixing Layer", Theoret. Comput. Fluid Dynamics, pp. 403-420, 2002, vol. 15.